Robust monolithic ultraviolet interferometer for the SHIMMER instrument on STPSat-1

John M. Harlander, Fred L. Roesler, Christoph R. Englert, Joel G. Cardon, Robert R. Conway, Charles M. Brown, and Jeff Wimperis

We describe the design, fabrication, and testing of a monolithic interferometer consisting entirely of optically contacted fused-silica optical elements that are assembled, adjusted, and permanently bonded in place. The interferometer is part of a spatial heterodyne spectrometer (SHS) [SHIMMER (Spatial Heterodyne Imager for Mesospheric Radicals)] that will be used for near-ultraviolet high-spectral-resolution limb imaging of OH solar resonance fluorescence from low Earth orbit aboard the satellite STPSat-1 scheduled for launch in 2006. The stability of the monolith coupled with the relaxed tolerances on optical quality and alignment inherent to SHS make this new instrument extremely robust and especially attractive for applications in harsh environments. © 2003 Optical Society of America

OCIS codes: 300.6300, 280.1310, 120.6200.

1. Introduction

For diffuse source spectroscopy over a limited spectral band, interferometric spectroscopy offers many advantages over conventional grating instruments; however, the subwavelength optical flatness, alignment, and stability required by interferometers have been technological barriers to their deployment for harsh environments. With these characteristics in mind we have been developing an unusual and novel interference spectroscopic technique called spatial heterodyne spectroscopy (SHS). SHS is an interferometric Fourier-transform technique, but unlike conventional Fourier-transform (FT) spectroscopy it requires no moving parts to obtain a spectrum. This feature has enabled the development of the first monolithic SHS interferometer consisting of fused-silica optical elements that are optically contacted, i.e., permanently bonded in place without use of an adhesive. Once the monolithic interferometer is successfully assembled, it is essentially one piece of glass, which makes it extremely robust, nearly impossible to misalign, much less massive, and smaller than a system employing mechanical mounts.

The monolithic interferometer was specifically developed to measure atmospheric OH (hydroxyl) solar resonance fluorescence near 308 nm from space. It is currently being integrated at the U.S. Naval Research Laboratory (NRL) into the Spatial Heterodyne Imager for Mesospheric Radicals (SHIMMER) instrument that is scheduled for launch on STPSat-1 in March 2006. SHIMMER STPSat-1 is the second in a series of instruments designed for atmospheric OH measurements. The first-generation SHIMMER instrument, which did not utilize a monolithic interferometer, flew as a Middeck experiment on Space Shuttle STS-112 in October 2002. This instrument, along with a more detailed description of SHS, is described elsewhere.[1] The scientific heritage of all SHIMMER instruments is provided by the highly successful flights of NRL's Middle Atmosphere High Resolution Spectrograph Investigation (MAHRSI) on the Cryogenic Infrared Spectrometers and Telescopes for the Atmosphere-Shuttle Pallet Satellite platform placed into orbit and returned by the Space Shuttle on STS-66 and STS-85 during November 1994 and August 1997.[2]

J. M. Harlander (harlander@stcloudstate.edu) is with the Department of Physics, Astronomy and Engineering Science, St. Cloud State University, 720 Fourth Avenue South, Mail Stop 315, St. Cloud, Minnesota 56301. F. L. Roesler is with the Department of Physics, 1150 University Avenue, University of Wisconsin-Madison, Madison, Wisconsin 57306. C. R. Englert, J. G. Cardon, R. R. Conway, and C. M. Brown are with the U.S. Naval Research Laboratory, Space Science Division Code 7641, 4555 Overlook Avenue SW, Washington, D.C. 20375. At the time of this research, J. Wimperis was with Wave Precision, 39 Auriga Drive, Ottawa, Ontario K2E 7Y8, Canada and is now with Light Machinery, Incorporated, 272 Spring Street, Almonte, Ontario K0A 1A0, Canada.

Received 2 August 2002; revised manuscript received 2 December 2002.

0003-6935/03/152829-06$15.00/0

Report Documentation Page

Form Approved
OMB No. 0704-0188

1. REPORT DATE	2. REPORT TYPE	3. DATES COVERED
02 DEC 2002		**00-00-2002 to 00-00-2002**

4. TITLE AND SUBTITLE	5a. CONTRACT NUMBER
Robust monolithic ultraviolet interferometer for the SHIMMER instrument on STPSat-1	5b. GRANT NUMBER
	5c. PROGRAM ELEMENT NUMBER
6. AUTHOR(S)	5d. PROJECT NUMBER
	5e. TASK NUMBER
	5f. WORK UNIT NUMBER
7. PERFORMING ORGANIZATION NAME(S) AND ADDRESS(ES) **Naval Research Laboratory,Space Science Division Code 7641,4555 Overlook Avenue SW,Washington,DC,20375**	8. PERFORMING ORGANIZATION REPORT NUMBER
9. SPONSORING/MONITORING AGENCY NAME(S) AND ADDRESS(ES)	10. SPONSOR/MONITOR'S ACRONYM(S)
	11. SPONSOR/MONITOR'S REPORT NUMBER(S)

12. DISTRIBUTION/AVAILABILITY STATEMENT
Approved for public release; distribution unlimited

13. SUPPLEMENTARY NOTES

14. ABSTRACT

15. SUBJECT TERMS

16. SECURITY CLASSIFICATION OF:			17. LIMITATION OF ABSTRACT	18. NUMBER OF PAGES	19a. NAME OF RESPONSIBLE PERSON
a. REPORT	b. ABSTRACT	c. THIS PAGE			
unclassified	**unclassified**	**unclassified**	**Same as Report (SAR)**	**6**	

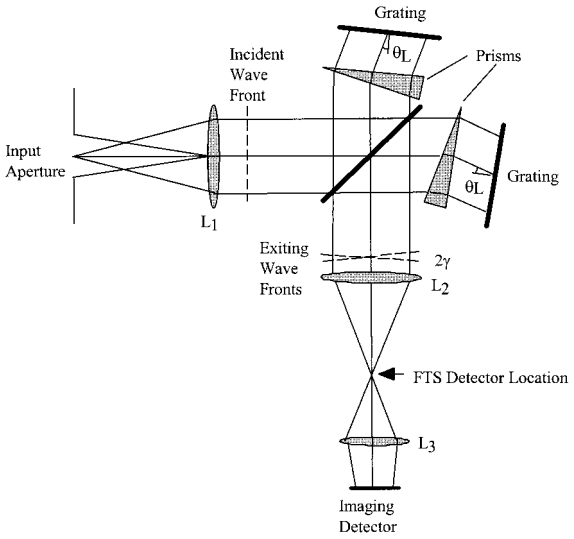

Fig. 1. Schematic diagram of the SHS configuration. For each wavelength in the incident wave front, two wave fronts exit the interferometer with a wavelength-dependent crossing angle between them. This produces a superposition of Fizeau fringes with wavelength-dependent spatial frequencies localized near the gratings and imaged on the detector. The image is the Fourier transform of the input spectrum about the heterodyne wavelength (the wavelength producing parallel output wave fronts). The prism angles are chosen so that, from a geometrical-optics point of view, the gratings appear coincident when viewed from the imaging detector. The Fourier-transform spectroscopy (FTS) detector location integrates the signal over the full aperture of the interferometer.

The advantages of interference spectrometers for space-based remote sensing are numerous. Interferometers can achieve sensitivities typically 100 times those of conventional grating instruments of similar size and spectral resolution. In addition, when used at high spectral resolution they do not require a long focal-length element to image a slit onto a detector pixel of typical size (~0.020 mm). As a result, interferometers can be made small and lightweight and still achieve a level of performance equal or superior to grating instruments of practical dimensions. To achieve even higher sensitivity (~100 times), SHS instruments can be field widened without moving parts, avoiding the mechanical mechanisms associated with conventional field-widened FT spectrometers. At UV wavelengths, SHS instruments are more practical than Fabry–Perot spectrometers (FPSs) because of their relaxed tolerances on element flatness, reduced sensitivity to coating absorption, and the ability to correct for interferometer defects and misalignments in data analysis.

2. Concept of Spatial Heterodyne Spectroscopy

In this section we summarize the basic features of SHS that have been discussed in greater detail elsewhere.[1,3] In SHS, Fizeau fringes of wavelength-dependent spatial frequency are produced by a modified Michelson interferometer in which the return mirrors are replaced by conventional diffraction gratings (see Fig. 1). The fringes, localized near the gratings, are recorded on a position-sensitive detector (e.g., CCD) and Fourier transformed to recover the spectrum. Zero spatial frequency corresponds to the Littrow wavelength, which can be chosen by adjustment of the gratings. As a result high-resolution spectra over a limited spectral range can be achieved with only modest requirements on the spatial resolution of the detector. In this process no element is mechanically scanned, which enables the implementation of the monolithic concept.

SHS achieves a maximum resolving power equal to the theoretical resolving power of the dispersive (grating plus prism) system whereas its field of view is characteristic of interferometric spectrometers. Furthermore, fixed field-widening prisms can be placed in the arms of the interferometer (see Fig. 1) that enable SHS instruments to view even larger fields without degrading the resolving power. If the fringe pattern is imaged by N pixels in the dimension parallel to Fig. 1, the bandwidth at the Nyquist limit is $N\lambda/2R$ where R is the resolving power. An interference filter can be used to eliminate aliasing and multiplex noise from out-of-band light. Depending on the detector and optics before the interferometer, zero, one, or two dimensions of spatial information can be recorded.[1]

SHS instruments have greatly relaxed alignment and surface figure tolerances when compared with scanning FT spectrometers and FPSs. A detector located at the focal plane of lens L_2 in Fig. 1 integrates the signal from the full aperture of the interferometer. In this case misalignments or figure errors in the interferometer of approximately one wavelength will greatly reduce the contrast of the fringes and degrade the signal-to-noise ratio of the spectrum. In SHS, the interferometer elements are nearly imaged on the detector resulting in each detector pixel integrating over a small area in the interferometer (see Fig. 3). Misalignments of a few wavelengths result in only a shift in the Littrow wavelength and do not reduce the fringe contrast. This feature of SHS also results in relaxed interferometer surface figure tolerances. Figure errors on the gratings, prisms, and beam splitter or index of refraction nonhomogeneities, if present, distort the Fizeau fringe patterns but do not reduce their contrast as long as the optical quality of the elements is good over the small area sampled by a detector pixel. A calibration image in monochromatic light provides a measure of the phase errors that can be used in software to correct broadband interferograms with minimal impact on the signal-to-noise ratio in the recovered spectrum.[4] In situations where an absolute wavelength reference is either not required or provided by the data, this aspect makes SHS much less sensitive to thermal drifts because, with each exposure, the interferometric alignment is recorded by the detector. Thermally induced changes in fringe phase and frequency can be dealt with easily in

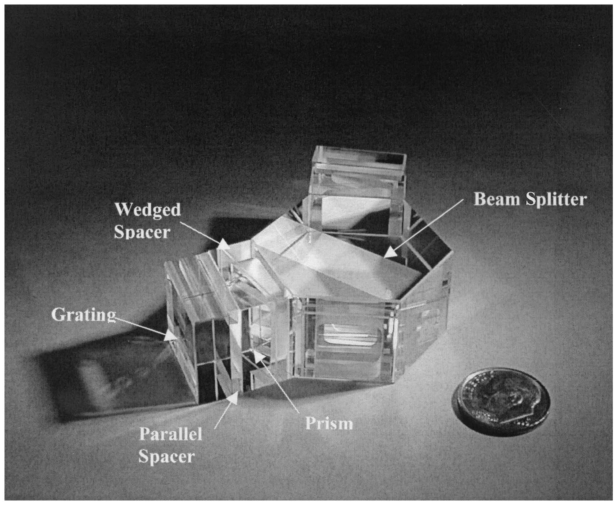

Fig. 2. Monolithic SHS interferometer. The beam splitter (the central hexagonal section) faces are 20 mm × 20 mm. Working outward in each arm the first elements are wedged spacers that mate the beam-splitter faces to the field-widening prisms. Parallel spacers mate the prisms to the gratings.

Table 1. Monolithic Interferometer Design Parameters

Parameter	Value
Resolving power	26,500
Grating	Etched holographic
Active area	10 mm × 10 mm
Groove density	1200 l/mm
Prisms	Homosil 13.02° wedge 5.0 mm thick
Field of view	10° at gratings
Beam splitter	Homosil zero-order path difference Hexagonal 20 mm × 20 mm faces
Spacers	Homosil
Beam splitter to prism	8.73° wedge 5.0 mm thick
Prism to grating	Plane parallel 2.0 mm thick
Coatings	
Antireflective	Quarter-wave MgF_2 on transmitting surfaces
Beam splitting	Multilayer dielectric nonpolarizing
Grating	Al with SiO_2 overcoat
Bandpass	3 nm (detector limited)
Field of view	Cone 10° full angle with no vignetting
Transmittance	>15%
Fabrication tolerances	
Littrow wavelength	307.1 ± 0.3 nm (±25 fringes)
Parallelism of fringes to grating grooves	Less than eight vertical fringes over 10-mm aperture

data reduction as long as the drift is slow compared with the time for a single exposure.

3. Monolithic Spatial Heterodyne Spectroscopy Interferometer

With support from NASA's Planetary Instrument Definition and Development Program (PIDDP) we developed the first monolithic SHS interferometer shown in Fig. 2. This design provides an elegant solution to the demanding requirement that interferometer optics (beam splitter, gratings, and prisms) be held to arcsecond angular tolerances and subwavelength linear tolerances during an exposure. Rather than use a complex and massive mechanical structure to hold the optics individually, they are optically contacted with fused-silica spacers between them. As a result the critical alignment between elements is maintained by the parts themselves instead of by an external mechanical assembly. Great care must be taken in the fabrication and assembly of the elements and spacers to achieve the required interferometric alignment; however, once successfully assembled, the monolithic interferometer is extremely robust, nearly impossible to misalign, much less massive, and smaller than a system employing mechanical mounts.

Most of the design parameters of the monolithic interferometer (prism and spacer angles, grating groove density) shown in Table 1 are the same as the Middeck SHIMMER instrument. These particular choices are explained in Harlander *et al.*[1] The primary difference between the two instruments is that the monolith has one quarter of the aperture area of the Middeck interferometer resulting in one quarter of the throughput and half of the resolving power. By making this choice, our intention was to make the instrument less massive and more compact. Also indicated in Table 1 are the design Littrow wavelength with its tolerance and the required parallelism of the fringes with respect to the grating grooves. As mentioned above, these requirements are greatly relaxed compared with the FT spectrometer and the FPS. Figure 3 shows a scale drawing of the monolithic interferometer. Chief rays at the center and edges of the field are indicated by solid lines whereas the dashed lines indicate the marginal rays of the point at the center of the field for a 10° cone angle. The intersection of this cone with the grating and prism indicates the small area over which the flatness of the surfaces must be of interferometric quality. Described in Sections 4 and 5 are the fabrication procedure and laboratory tests of the monolithic interferometer that demonstrate its near-theoretical performance.

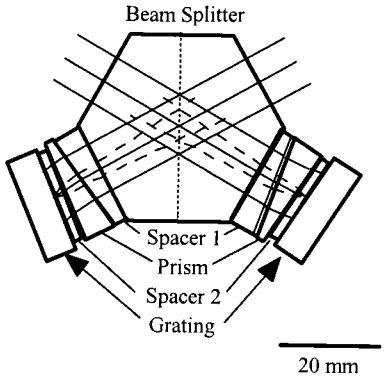

Fig. 3. Scale drawing of the monolithic interferometer. See text for details.

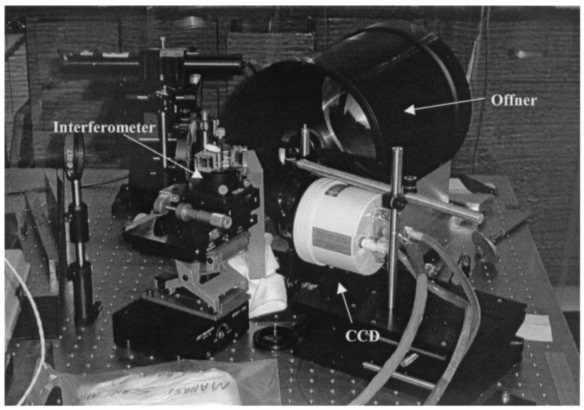

Fig. 4. Laboratory setup. The monolithic interferometer is on the laboratory jacks near the center of the image.

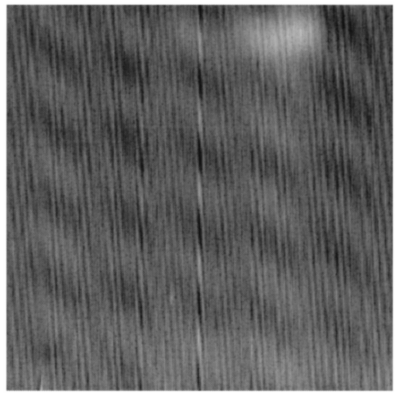

Fig. 5. MnNe fringe pattern. The horizontal direction is in the dispersion plane of the gratings.

4. Fabrication Issues

On the basis of their experience with optical contacting and the manufacture of field-widened Michelson interferometers,[5] Wave Precision, Inc. in Ottawa, Ontario, Canada, was selected for the fabrication and assembly of the monolith. The initial step in the fabrication was to machine and polish all sides of each part to arcsecond angular tolerances. The grating blanks were then sent to Spectragon, Ltd. (Sweden) to etch the holographic grating grooves. The gratings were etched over only the central 10 mm $\times$ 10 mm area of the 20 mm $\times$ 20 mm blank, which results in a nonetched area around the perimeter of the grating for optical contacting. After the beam-splitting coating was applied to one half of the hexagonal beam splitter, the halves were optically contacted, heat treated, and then hand polished until a zero-order white-light fringe was observed over the entire beam-splitter field. During assembly of the interferometer arms, alignment of the spacers, prisms, and gratings to the beam splitter was accomplished with the aid of a Zerodur plate onto which the bottom surface of the beam splitter was placed and aligned forming a Fizeau fringe field between the plate and the bottom of the beam splitter. As the parts were contacted to the beam splitter, the Fizeau fringe field between the plate and the bottom surfaces of the parts was monitored to ensure proper alignment to the beam splitter. After assembly the interferometer was removed from the plate, tested in the UV for fringe frequency, and baked at 200 °C overnight to further strengthen the optical contacts.

5. Optical Tests

The optical performance of the monolithic interferometer was tested in our laboratory for angular acceptance, Littrow wavelength, fringe contrast, and resolving power. Figure 4 shows the breadboard experimental setup used. Diffuse light enters the system through an entrance aperture and is collimated before entering the interferometer (shown near the middle of Fig. 4). The entrance aperture was chosen to produce a 10-deg cone angle inside the interferometer (see Table 1). Following the interferometer, light enters an Offner optical assembly, shown in the upper half of Fig. 4, that images the fringe pattern onto a CCD detector. The instrumental passband is limited to approximately 3 nm by an interference filter placed just before the CCD detector.

Figure 5 shows the fringe pattern that we obtained using a multiline MnNe hollow cathode lamp corrected for dark field, background, and flat field. We obtained a flat field for each arm by inserting a mask between the beam splitter and the prism into slots machined into the spacers. The image was cropped from a grating area of 10 mm $\times$ 10 mm to 9.23 mm $\times$ 9.23 mm to match the area that will be imaged on STPSat-1. The dispersion plane of the gratings is horizontal. The high-contrast band running vertically through image center is the location of zero path difference. Along this line the images of the gratings intersect on the detector, and all wave-front pairs have the same phase. The modulation ($\sim$5 fringes) along this band is due to a slight tilt of one of the interferometer arms in the plane perpendicular to Fig. 1 but is within the eight-fringe tolerance indicated in Table 1. The bright feature near the top right of the image is additive scattered light in the test setup. This light does not significantly affect the measured spectrum because it occurs at spatial frequencies that are much different from the spectral information. It does, however, slightly increase the shot noise in the interferogram and slightly decrease the signal-to-noise ratio in the spectrum. This illustrates another advantage of SHS over conventional grating spectroscopy: Scattered light occurring at frequencies unique from spectral information is naturally removed in the data analysis.

To obtain a MnNe spectrum, fringes shown in Fig. 5 were apodized with a Hanning function and two-dimensionally Fourier transformed. A slice from the transform is shown in Fig. 6. The wavelength scale was obtained by a least-squares fit to 17 known lines in the MnNe spectrum, 11 of which are shown in Fig. 6. The derived resolution of the system is 0.0127 nm corresponding to a resolving power of

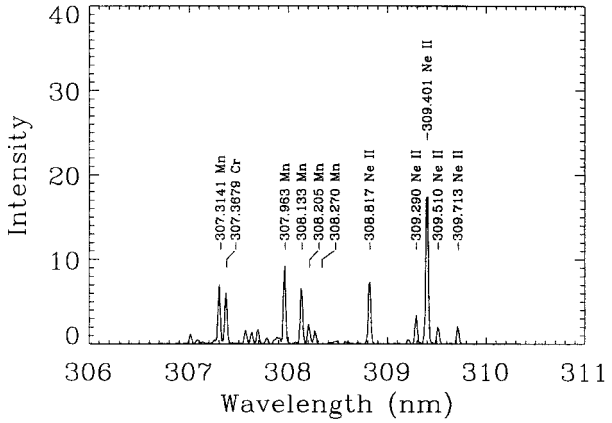

Fig. 6. MnNe spectrum. All the line positions were used to determine the Littrow wavelength and resolution; however, only the 11 brightest lines are labeled.

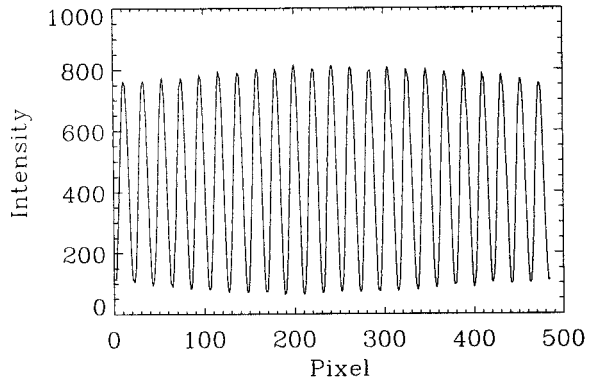

Fig. 8. Zn interferogram intensity slice. Note the high visibility of the fringes near the center of the interferogram where the path difference is zero.

24,500. The reduction in resolution of ~8% from the design value shown in Table 1 is consistent with the cropping applied to the fringe image. The Littrow wavelength determined by the least-squares fit is 307.291 nm, which is within the tolerance indicated in Table 1.

Figure 7 shows the fringe pattern (processed similarly to Fig. 5) that we obtained using a virtually monochromatic Zn lamp emission feature at 307.59 nm that was isolated with an interference filter. The straight fringes indicate the flatness of the optical surfaces and the homogeneity of the fused silica, whereas the near-uniform modulation across the image indicates that the Zn line is unresolved and more importantly that the fringe amplitude is not degraded by the large angular acceptance of the instrument. Figure 8 shows an intensity slice through a Zn lamp interferogram. The visibility $[(I_{max} - I_{min})/(I_{max} + I_{min})]$ of the fringe pattern at the center of the image (near zero path difference) is in excess of 0.85. Also evident in Fig. 8 is the decrease in visibility of the interferogram at the edges of the field where the path difference is largest. This decrease is due to the range of angles in the incident cone of light. Figure 9 shows the spectrum derived from the interferogram shown in Fig. 7. We did not apodize the interferogram prior to transforming, but it was zero filled to better illustrate the ringing in the wings of the line in the resulting spectrum. We performed the wavelength calibration using the data from Fig. 6.

6. Mechanical Tests

Once the monolithic interferometer is successfully assembled, the only risk is in the maintenance of the integrity of the optical contacts. Studies[6] have shown that both the tensile and the shear strength of such contacts exceed our requirements. To empirically test the strength of the optical contacts, we performed a successful qualification-level vibration test (12.3-g rms, three axis) on the interferometer integrated in its STPSat-1 flight fixture. We also performed successful thermal tests over the expected temperature range of STPSat-1 on an optically contacted part with size, mass, and contact area similar to the actual interferometer.

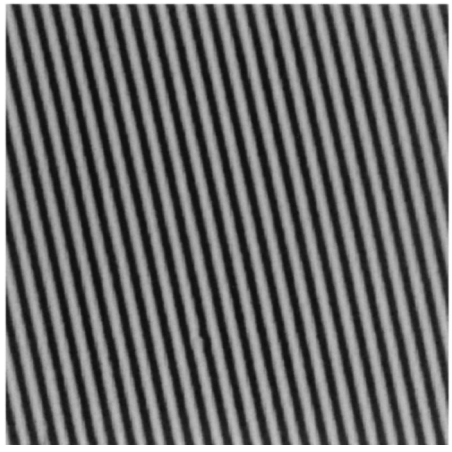

Fig. 7. Zn emission line interferogram (λ = 307.59 nm).

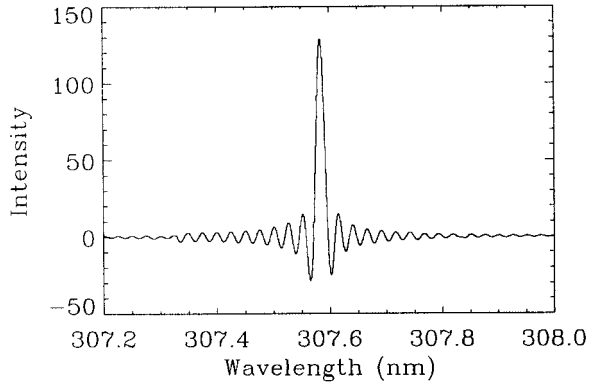

Fig. 9. Zn emission line spectrum. No apodization function, but zero filling was applied to the interferogram before transforming, which results in the ringing in the wings of the line.

7. Future Missions

Several SHS instruments are being developed at NRL for launch in the next few years. The first orbital flight of a SHS instrument to study OH solar resonance fluorescence occurred with the launch of SHIMMER Middeck aboard STS-112 in the fall of 2002. Although this instrument does not include a monolithic interferometer, it will provide valuable data to help guide the development of SHS instruments and analysis routines for future missions in addition to providing a limited atmospheric OH data set. The monolithic interferometer described in this paper is scheduled for launch on STPSat-1 in March 2006. SHIMMER STPSat-1 will view the Earth's limb over the tropics and subtropics for at least one year. The next-generation monolithic SHS instrument will be part of the Aeronomy of Ice in the Mesophere (AIM) satellite recently selected as a Small Explorer by NASA. AIM consists of a suite of four instruments in a Sun-synchronous noon–midnight polar orbit scheduled for launch in September 2006 with the objective of studying why polar mesospheric clouds form and why they vary.

Funding for this research was provided by NASA's PIDDP program (NRA 97-OSS-10 PIDDP). The SHIMMER Middeck and SHIMMER STPSat-1 missions are a joint effort between the U.S. Department of Defence Space Test Program (Air Force Space and Missile Systems Center/Space Test Programs Office) and the NRL. Additional support for SHIMMER Middeck has been provided by the National Science Foundation (ATM-9612228) and NASA G/LCAS (NRA 00-OSS-01 G/LCAS).

References

1. J. M. Harlander, F. L. Roesler, J. G. Cardon, C. R. Englert, and R. R. Conway, "SHIMMER: a spatial heterodyne spectrometer for remote sensing of Earth's middle atmosphere," Appl. Opt. **41,** 1343–1352 (2002).
2. R. R. Conway, M. H. Stevens, C. M. Brown, J. G. Cardon, S. E. Zasadil, and G. H. Mount, "The Middle Atmosphere High Resolution Spectrograph investigation," J. Geophys. Res. **104D,** 16327–16348 (1999).
3. J. M. Harlander, R. J. Reynolds, and F. L. Roesler, "Spatial heterodyne spectroscopy for the exploration of diffuse interstellar emission lines at far ultraviolet wavelengths," Astrophys. J. **396,** 730–740 (1992).
4. J. M. Harlander, H. T. Tran, F. L. Roesler, K. P. Jaehnig, S. M. Seo, W. T. Sanders, and R. J. Reynolds, "Field-widened spatial heterodyne spectroscopy: correcting for optical defects and new vacuum ultraviolet performance tests," in *EUV, X-Ray and Gamma-Ray Instrumentation of Astronomy V*, O. E. Siegmund and J. Vallerga, eds., Proc. SPIE **2280,** 310–319 (1994).
5. W. A. Gault, S. Brown, A. Moise, D. Liang, G. Sellar, G. G. Sheperd, and J. Wimperis, "ERWIN: an E-region wind interferometer," Appl. Opt. **35,** 2913–2922 (1996).
6. H. H. Karow, *Fabrication Methods for Precision Optics* (Wiley, New York, 1993).